RSC Advances

PAPER

View Article Online
View Journal | View Issue

Cite this: *RSC Adv.*, 2017, **7**, 44706

Microstructure and sintering behavior of low temperature cofired $Li_{4/5}Mg_{4/5}Ti_{7/5}O_4$ ceramics containing $BaCu(B_2O_5)$ and TiO_2 and their compatibility with a silver electrode†

Huanfu Zhou,* Xianghu Tan, Kangguo Wang, Wendong Sun, Hong Ruan and Xiuli Chen

Received 29th June 2017
Accepted 8th September 2017

DOI: 10.1039/c7ra07203a

rsc.li/rsc-advances

$Li_{4/5}Mg_{4/5}Ti_{7/5}O_4$ (LMT) ceramics were prepared *via* a solid-state reaction method. The LMT ceramics, sintered at 1100 °C, presented good microwave dielectric properties with $\varepsilon_r = 22.8$, $Q \times f = 100\,000$ GHz and $\tau_f = -15.0$ ppm °C^{-1}. $BaCu(B_2O_5)$ (BCB) was added to lower the sintering temperature of the ceramics. The addition of BCB reduced the sintering temperature, but slightly degraded the microwave dielectric properties of the LMT ceramics. The 0.97LMT–0.03BCB ceramic showed a low sintering temperature of 900 °C and good microwave dielectric properties with an appropriate ε_r of 20.9, high $Q \times f$ of 42 104 GHz and negative τ_f of −24.0 ppm °C^{-1}. TiO_2 was added to improve the ε_r and adjust the τ_f value. The 0.85(0.97LMT–0.03BCB)–0.15TiO_2 ceramic, sintered at 875 °C, showed good dielectric properties, with a high $Q \times f$ of 37 700 GHz, appropriate ε_r of 23.1 and near-zero τ_f of −5.9 ppm °C^{-1}. Obviously, the 0.85(0.97LMT–0.03BCB)–0.15TiO_2 ceramic is a good candidate for low temperature co-fired ceramic devices.

1. Introduction

Recently, low temperature co-fired ceramic (LTCC) technology has been widely used in the large-scale integration of microwave dielectric devices.[1–4] In LTCCs, the microwave dielectric materials must be sintered at a temperature below the melting point of Ag (961 °C). Furthermore, the materials should have excellent microwave dielectric properties (a high quality factor, an appropriate permittivity and a near-zero temperature coefficient of resonant frequency) and good chemical compatibility with Ag.[5–8] A huge number of ceramics with the AB_2O_4 spinel structure have been reported to exhibit good microwave dielectric properties, such as $Li_2MgTi_3O_8$,[9] Mg_2TiO_4[10] and Li_2MgTiO_4.[11] However, their high sintering temperatures have limited their further application to LTCC devices. Therefore, many researchers are trying to lower the sintering temperatures of microwave dielectric ceramics. Sintering aids, super-fine powders and low melting point materials have all been used to realize low temperature sintering of ceramics.[12–14] The addition of sintering aids can degrade the microwave dielectric properties of the ceramics, but do not increase their production cost. Using super-fine powders increases the production cost, but does not decrease the performance. It is difficult to find a new low melting point material.

In this paper, $Li_{4/5}Mg_{4/5}Ti_{7/5}O_4$ (LMT) spinel ceramics were designed to obtain new microwave dielectric materials with good properties. The phase composition, microstructure and microwave dielectric properties of $Li_{4/5}Mg_{4/5}Ti_{7/5}O_4$ (LMT) spinel ceramics were studied. LMT ceramics exhibit high sintering temperatures, which restrict their further application. In order to control the production cost, the method of adding sintering aids has been widely adopted to lower the sintering temperature of LMT ceramics. Zhou *et al.*[15] reported that the addition of $BaCu(B_2O_5)$ (BCB) could lower the sintering temperature of ceramics. Their $Ba_3Ti_5Nb_6O_{28}$ ceramic, containing 5.0 wt% BCB and sintered at 925 °C, exhibited good microwave dielectric properties of $Q \times f = 19\,191$ GHz, $\varepsilon_r = 38.2$ and $\tau_f = 12$ ppm °C^{-1}. Therefore, in this study, BCB was added to LMT ceramics to lower their sintering temperatures, and the effects of BCB on the sintering temperature and microwave dielectric properties of the ceramics are discussed herein. Furthermore, TiO_2 was added to the LMT ceramics to improve their permittivity and adjust the temperature coefficient of resonant frequency to near-zero. The effects of TiO_2 addition on the phase composition and microwave dielectric properties of the LMT + BCB ceramics were also examined.

Guangxi Ministry-Province Jointly-Constructed Cultivation Base for State Key Laboratory of Processing for Non-ferrous Metal and Featured Materials, Guangxi Key Laboratory in Universities of Clean Metallurgy and Comprehensive Utilization for Non-ferrous Metals Resources, Collaborative Innovation Center for Exploration of Hidden Nonferrous Metal Deposits and Development of New Materials in Guangxi, School of Materials Science and Engineering, Guilin University of Technology, Guilin 541004, China. E-mail: zhouhuanfu@163.com

† Electronic supplementary information (ESI) available. See DOI: 10.1039/c7ra07203a

2. Experimental procedure

LMT ceramics were prepared *via* a conventional solid-state reaction method using high purity powers of Li_2CO_3 (≥99%), MgO (≥99%) and TiO_2 (≥99%). The raw materials were stoichiometrically weighed and ball milled with zirconia balls in alcohol medium for 4 h. The mixtures were then rapidly dried and calcined at 900 °C for 4 h. The high purity powders (≥99%) of $Ba(OH)_2 \cdot 8H_2O$, CuO and H_3BO_3 were used to prepare the BCB powders. The powders were stoichiometrically weighed, mixed, dried and calcined at 800 °C for 4 h. The LMT powders were mixed with different amounts of BCB for 4 h, and then part of the 0.97LMT–0.03BCB powders were mixed with different levels of TiO_2 for 4 h. The $(1-x)$LMT–xBCB($0 \le x \le 0.04$) and $(1-y)$[0.97LMT–0.03BCB]–$y$$TiO_2$ ($0.05 \le y \le 0.20$) powders were granulated with 5 wt% polyvinyl alcohol (PVA) and pressed into disks of 12 mm in diameter and 6 mm in thickness using a uniaxial pressure of ~200 MPa. Finally, the disks were sintered in the temperature range of 825–1025 °C for 4 h.

The crystalline phases of the samples were identified using X-ray diffraction (XRD) with Cu K_α radiation generated at 40 kV and 40 mA (Model X'Pert PRO, PANalytical, Almelo, Holland). The surface morphology of the ceramics was studied using scanning electron microscopy (SEM) (Model JSM6380-LV SEM, JEOL, Tokyo, Japan). The bulk density of the sintered ceramics was tested using the Archimedes method. Dielectric behaviors at microwave frequencies were measured using the $TE_{01\delta}$ shielded cavity method on a Network Analyzer (Model N5230A, Agilent Co., CA, 10 MHz to 40 GHz). The temperature coefficients of resonant frequency (τ_f) were measured using the open cavity method with an invar cavity in a temperature chamber (DELTA9039, Delta Design, USA). The τ_f values were calculated using the following formula:

$$\tau_f = \frac{f_T - f_0}{f_0(T - T_0)} \quad (1)$$

where f_T and f_0 are the resonant frequencies at temperatures T (85 °C) and T_0 (25 °C), respectively.

3. Results and discussion

3.1 Phase structure and microwave dielectric properties of LMT ceramics

Fig. 1 presents the XRD patterns of the LMT ceramics sintered at different temperatures. It can be seen that all the observed peaks were indexed according to $Li_2MgTi_3O_8$ (PDF: 00-048-0263). The reasons for this phenomenon are as follows. Firstly, $LiMg_{1/2}Ti_{3/2}O_4$ and Mg_2TiO_4 might be formed according to the following reaction mechanism: $0.4Li_2CO_3 + 0.8MgO + 1.4TiO_2 \rightarrow 0.8LiMg_{1/2}Ti_{3/2}O_4 + 0.4CO_2 + 0.2Mg_2TiO_4$. It is worth noting that the cation sizes of $LiMg_{1/2}Ti_{3/2}O_4$ and Mg_2TiO_4 are similar, and the mismatch (∇r) was calculated as 1.2% (≤15%). Furthermore, $LiMg_{1/2}Ti_{3/2}O_4$ and Mg_2TiO_4 had a similar structure (spinel structure).[16,17] Therefore, 1/2Li,1/4Mg,1/4Ti could be replaced with Mg, and LMT solid solution might be formed according to the following reaction mechanism: $0.8LiMg_{1/2}Ti_{3/2} + 0.2Mg_2TiO_4 \rightarrow Li_{4/5}Mg_{4/5}Ti_{7/5}O_4$. The SEM micrographs of the

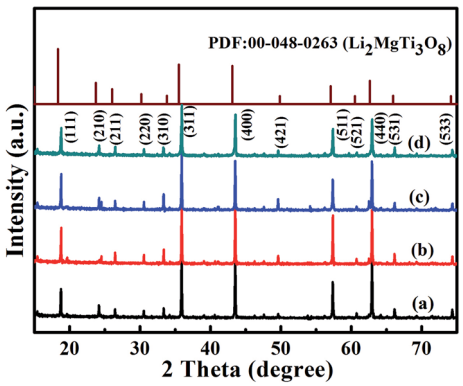

Fig. 1 Room-temperature XRD patterns of the LMT ceramics sintered at (a) 1050 °C, (b) 1075 °C, (c) 1100 °C and (d) 1125 °C.

LMT ceramics are shown in Fig. S1.† With increasing the sintering temperature from 1050 °C to 1100 °C, the merging of the small grains gave rise to larger grains and eliminated the pores, leading to an increased average grain size and decreased porosity. By further increasing the sintering temperature, the average grain size increased, because grains continued to arise. On the other hand, the velocity of the grain boundary was too fast when the sintering temperature was too high, making the elimination of pores difficult,[18,19] so the porosity increased. The change in porosity resulted in a change of the bulk density.

Fig. 2 illustrates the bulk density (ρ), permittivity (ε_r) and quality factor ($Q \times f$) of the LMT ceramics sintered at different temperatures. The ρ of the LMT ceramics firstly increased and then decreased with increasing the sintering temperature. The change of the ε_r and $Q \times f$ of the LMT ceramics as a function of the sintering temperature showed a trend similar to that of the ρ, showing that the relative density had a crucial effect on the ε_r and $Q \times f$. The LMT ceramics sintered at 1100 °C possessed good microwave dielectric properties with a high $Q \times f$ of 100 000 GHz, an appropriate ε_r of 22.8 and a negative τ_f of −15 ppm $°C^{-1}$. The high sintering temperature limited the further application of LMT in LTCC devices, so $BaCu(B_2O_5)$ (BCB) was chosen to reduce the sintering temperature of the ceramics.

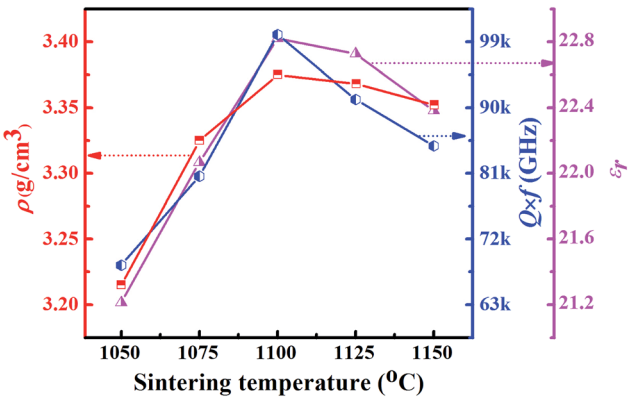

Fig. 2 The bulk density (ρ), permittivity (ε_r) and $Q \times f$ values of the LMT ceramics as a function of their sintering temperatures.

3.2 The effects of BCB addition on the sintering temperature and microwave dielectric properties of LMT ceramics

Fig. S2† shows the room-temperature XRD patterns of the $(1-x)$LMT–xBCB ($0.01 \le x \le 0.04$) ceramics. The XRD patterns of all components were similar to that of LMT, and all observed peaks of $(1-x)$LMT–xBCB were indexed according to $Li_2MgTi_3O_8$ (PDF: 00-048-0263). Due to the low content of BCB in the $(1-x)$LMT–xBCB ceramics, it could not be detected using XRD. Fig. S3† presents the SEM micrographs of the $(1-x)$LMT–xBCB ceramics. The porosity increased and the average grain size decreased with increasing BCB content, which illustrates that the addition of BCB played a key role in changing the microstructure of the $(1-x)$LMT–xBCB ceramics.

The ρ, ε_r and $Q \times f$ of the $(1-x)$LMT–xBCB ceramics as a function of the sintering temperature are illustrated in Fig. 3. The ρ, ε_r and $Q \times f$ of the $(1-x)$LMT–xBCB ceramics first increased and then decreased with increasing sintering temperature. With increasing the BCB content, the sintering temperature of the $(1-x)$LMT–xBCB ceramics gradually decreased, because BCB has a low sintering temperature (~810 °C). With increasing the BCB content, the ρ of the $(1-x)$LMT–xBCB ceramics slowly decreased, because the porosity of the $(1-x)$LMT–xBCB ceramics increased. The phase composition has a great effect on the microwave dielectric properties of multiphase systems.[20,21] Compared with LMT, BCB has relatively poor microwave dielectric properties, with ε_r of 7.4, $Q \times f$ of 50 000 GHz and τ_f of −32 ppm °C^{-1}.[22] Therefore, the ε_r decreased from 21.1 to 20.9 and $Q \times f$ decreased from 58 807 GHz to 30 405 GHz. Table 1 shows that the τ_f decreased from −17.3 ppm °C^{-1} to −28.5 ppm °C^{-1} with increasing BCB content. The addition of BCB lowered the sintering temperature but also deteriorated the microwave dielectric properties of the ceramics. In particular, the 0.97LMT–0.03BCB ceramics showed a low sintering temperature of 900 °C and good microwave dielectric properties with an appropriate ε_r of 20.9, a high $Q \times f$ of 42 104 GHz and a more negative τ_f of −24.0 ppm °C^{-1}. In order to adjust the τ_f of the 0.97LMT–0.03BCB ceramic, $(1-y)$[0.97LMT–0.03BCB]–yTiO$_2$ (y = 0.05, 0.10, 0.15, 0.20) systems were designed.

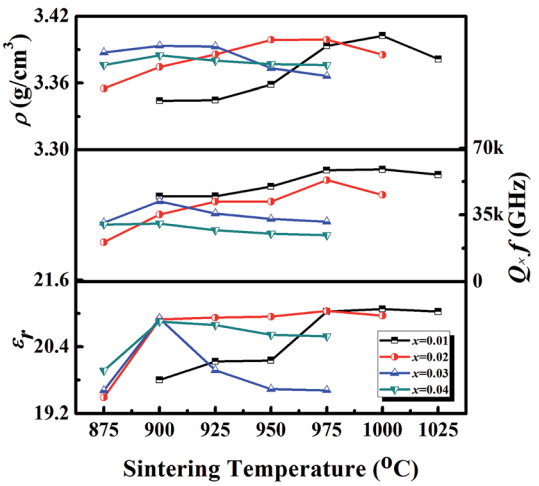

Fig. 3 The bulk density (ρ), permittivity (ε_r) and $Q \times f$ values of the $(1-x)$LMT–xBCB ceramics as a function of their sintering temperatures.

Table 1 The τ_f values of $(1-x)$LMT–xBCB (x = 0.01, 0.02, 0.03, 0.04) and $(1-y)$[0.97LMT–0.03BCB]–yTiO$_2$ (y = 0.05, 0.10, 0.15, 0.20) ceramics sintered at their optimum temperatures

Condition		The optimum sintering temperature (°C)	τ_f (ppm °C^{-1})
$(1-x)$LMT–xBCB	$x = 0$	1100	−15.0
	$x = 0.01$	1000	−17.3
	$x = 0.02$	975	−20.5
	$x = 0.03$	900	−24.0
	$x = 0.04$	900	−28.5
$(1-y)$[0.97LMT–0.03 BCB]–yTiO$_2$	$y = 0.05$	875	−21.1
	$y = 0.10$	875	−9.6
	$y = 0.15$	875	−5.9
	$y = 0.20$	900	−15.0

3.3 The effects of TiO_2 addition on the sintering temperature and microwave dielectric properties of LMT + BCB ceramics

The room-temperature XRD patterns of the $(1-y)$[0.97LMT–0.03BCB]–yTiO$_2$ (y = 0.05, 0.10, 0.15, 0.20) ceramics are shown in Fig. 4(a). When y = 0.05–0.15, all XRD patterns agreed well with those of $Li_2MgTi_3O_8$ (PDF: 00-048-0263) and $MgTiO_3$ (PDF: 01-079-0831), and no other phases could be detected. When y = 0.05, the composition was $(1-z)LiMg_{1/2}Ti_{3/2}O_4$–$zMg_2TiO_4$ as a solid solution and $MgTiO_3$ might be formed according to the following reaction mechanism: $Mg_2TiO_4 + TiO_2 \rightarrow 2MgTiO_3$. When y = 0.10 or 0.15, Mg_2TiO_4 disappeared and $Li_{4/3}Ti_{5/3}O_4$ appeared. $LiMg_{1/2}Ti_{3/2}O_4$ and $Li_{4/3}Ti_{5/3}O_4$ had similar crystal structures and ionic radii, so these compounds could form solid solutions. The composition was $(1-m)LiMg_{1/2}Ti_{3/2}O_4$–$mLi_{4/3}Ti_{5/3}O_4$ as a solid solution. When y = 0.20, the diffraction peak of the $MgTi_2O_5$ (PDF: 00-020-0694) phase at lower angle regions of 20–30° was observed, due to the addition of excessive TiO_2. $MgTi_2O_5$ may be formed according to the following reaction mechanism: $MgTiO_3 + TiO_2 \rightarrow MgTi_2O_5$.

Fig. 4(b) and (c) show the ternary phase diagrams of the Li_2O–MgO–TiO_2 systems and the enlarged patterns of the Mg_2TiO_4–$MgTi_2O_5$–$Li_{4/3}Ti_{5/3}O_4$ concentration triangle, respectively. The ternary phase diagrams were used to identify the change in phase composition. The group point moved along the red line, dashed to the TiO_2 point with increasing TiO_2 content. When y = 0 or 0.05, the group point was located in the $MgTiO_3$–$LiMg_{1/2}Ti_{3/2}O_4$–Mg_2TiO_4 concentration triangle. With increasing y value, the group point is far away from the Mg_2TiO_4 and $LiMg_{1/2}Ti_{3/2}O_4$ points but closer to the $MgTiO_3$ point, indicating that the relative content of Mg_2TiO_4 and $LiMg_{1/2}Ti_{3/2}O_4$ decreased, but the relative content of $MgTiO_3$ increased. Furthermore, compared with the Mg_2TiO_4 point, the group point was closer to the $LiMg_{1/2}Ti_{3/2}O_4$ point, which indicates that the relative content of Mg_2TiO_4 decreased in $(1-z)LiMg_{1/2}Ti_{3/2}O_4$–$zMg_2TiO_4$. Because the relative content of Mg_2TiO_4, with a large ionic

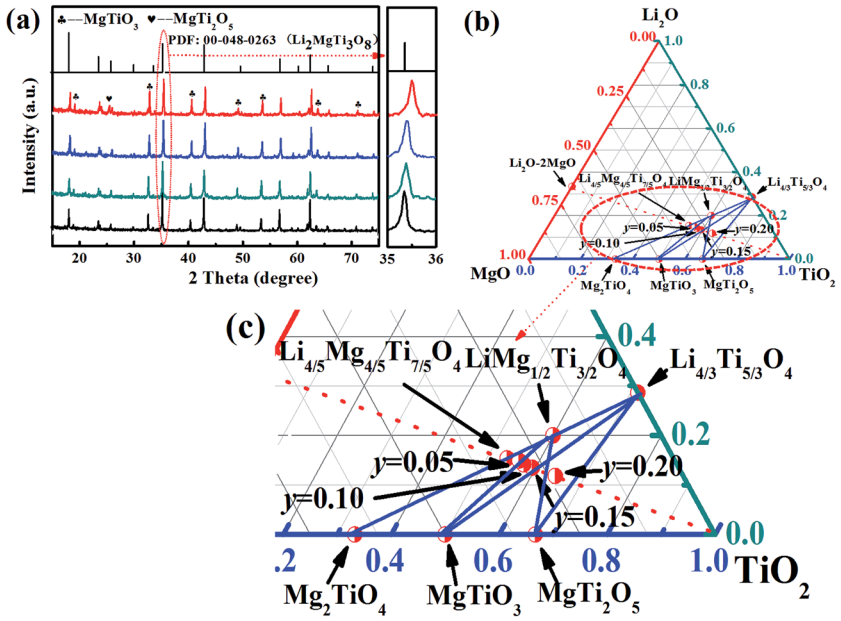

Fig. 4 (a) Room-temperature XRD patterns of the $(1-y)$[0.97LMT–0.03BCB]–yTiO$_2$ (y = 0.05, 0.10, 0.15, 0.20) ceramics. (b) Ternary phase diagrams of Li$_2$O–MgO–TiO$_2$ systems. (c) Enlarged patterns of the Mg$_2$TiO$_4$–MgTi$_2$O$_5$–Li$_{4/3}$Ti$_{5/3}$O$_4$ concentration triangle.

radius, decreased in $(1-z)$LiMg$_{1/2}$Ti$_{3/2}$O$_4$–zMg$_2$TiO$_4$, the unit cell parameters of $(1-z)$LiMg$_{1/2}$Ti$_{3/2}$O$_4$–zMg$_2$TiO$_4$ decreased. When y = 0.10 and 0.15, the group point was located in the MgTiO$_3$–LiMg$_{1/2}$Ti$_{3/2}$O$_4$–Li$_{4/3}$Ti$_{5/3}$O$_4$ concentration triangle. With increasing y value, the group point is far away from the LiMg$_{1/2}$Ti$_{3/2}$O$_4$ point but closer to the Li$_{4/3}$Ti$_{5/3}$O$_4$ point and MgTiO$_3$ point, indicating that the relative content of LiMg$_{1/2}$Ti$_{3/2}$O$_4$ decreased, but the relative content of MgTiO$_3$ and Li$_{4/3}$Ti$_{5/3}$O$_4$ increased. Compared with the LiMg$_{1/2}$Ti$_{3/2}$O$_4$ point, the group point was closer to the Li$_{4/3}$Ti$_{5/3}$O$_4$ point. When y = 0.20, the group point was located in the LiMg$_{1/2}$Ti$_{3/2}$O$_4$–Li$_{4/3}$Ti$_{5/3}$O$_4$–MgTi$_2$O$_5$–MgTiO$_3$ concentration quadrilateral, implying the formation of MgTi$_2$O$_5$. Furthermore, the group point continued to approach the Li$_{4/3}$Ti$_{5/3}$O$_4$ point for the LiMg$_{1/2}$Ti$_{3/2}$O$_4$–Li$_{4/3}$Ti$_{5/3}$O$_4$ line. Because the relative content of Li$_{4/3}$Ti$_{5/3}$O$_4$, with a small ionic radius, increased in $(1-m)$LiMg$_{1/2}$Ti$_{3/2}$O$_4$–mLi$_{4/3}$Ti$_{5/3}$O$_4$, the unit cell parameters of $(1-m)$LiMg$_{1/2}$Ti$_{3/2}$O$_4$–mLi$_{4/3}$Ti$_{5/3}$O$_4$ decreased. Thus, LiMg$_{1/2}$Ti$_{3/2}$O$_4$ peaks shifted to high angles, as shown in Fig. 4(a).

The SEM micrographs of the $(1-y)$[0.97LMT–0.03BCB]–yTiO$_2$ (y = 0.05, 0.10, 0.15, 0.20) ceramics are given in Fig. S4.† Compared with the undoped-TiO$_2$ 0.97LMT–0.03BCB ceramic, the average grain size of the 0.95[0.97LMT–0.03BCB]–0.05TiO$_2$ ceramic was decreased, because the phase composition had changed as follows: [BCB and LMT solid solutions, y = 0] → [BCB, $(1-z)$LiMg$_{1/2}$Ti$_{3/2}$O$_4$–zMg$_2$TiO$_4$ solid solution and MgTiO$_3$, y = 0.05]. With increasing the amount of TiO$_2$ added from 0.05 to 0.20, the phase composition changed as follows: [BCB, $(1-z)$LiMg$_{1/2}$Ti$_{3/2}$O$_4$–zMg$_2$TiO$_4$ solid solution and MgTiO$_3$, y = 0.05] → [BCB, $(1-m)$LiMg$_{1/2}$Ti$_{3/2}$O$_4$–mLi$_{4/3}$Ti$_{5/3}$O$_4$ solid solution and MgTiO$_3$, y = 0.10 and 0.15] → [BCB, $(1-m)$LiMg$_{1/2}$Ti$_{3/2}$O$_4$–mLi$_{4/3}$Ti$_{5/3}$O$_4$ solid solution, MgTiO$_3$ and MgTi$_2$O$_5$, y = 0.20]. The average grain size of $(1-y)$[0.97LMT–0.03BCB]–yTiO$_2$ gradually increased, but the porosity of the ceramics first decreased and then increased. Overall, the density of the ceramics increased first and then decreased. Furthermore, the EDS analysis of the 0.85[0.97LMT–0.03BCB]–0.15TiO$_2$ ceramic is inserted in Fig. S4.† For "grain I", the atomic number ratio of Mg to Ti is close to 1 : 4, so "grain I" is the $(1-m)$LiMg$_{1/2}$Ti$_{3/2}$O$_4$–mLi$_{4/3}$Ti$_{5/3}$O$_4$ solid solution. For "grain II", the atomic number ratio of Mg to Ti is close to 1 : 1, so "grain II" is MgTiO$_3$. BCB grains could not be found due to the low content of BCB.

The ρ, ε_r and Q an$f$ of the $(1-y)$[0.97LMT–0.03BCB]–yTiO$_2$ ceramic as a function of the sintering temperature are demonstrated in Fig. 5. With increasing the sintering temperature, the ρ, ε_r and $Q \times f$ of the $(1-y)$[0.97LMT–0.03BCB]–yTiO$_2$ ceramic presented a similar trend. When the TiO$_2$ content was increased from 0 to 0.05, the phase composition changed from BCB and LMT solid solution to a BCB, $(1-z)$LiMg$_{1/2}$Ti$_{3/2}$O$_4$–zMg$_2$TiO$_4$ solid solution and MgTiO$_3$, and the bulk density and microwave dielectric properties of ceramics changed as follows: ($\rho \sim 3.39$ g cm^{-3}, $Q \times f \sim 42\,104$ GHz, $\varepsilon_r \sim 20.9$, and $\tau_f \sim -24.0$ ppm °C^{-1}) → ($\rho \sim 3.41$ g cm^{-3}, $Q \times f \sim 35\,300$ GHz, $\varepsilon_r \sim 21.9$, and $\tau_f \sim -21.1$ ppm °C^{-1}). When the amount of TiO$_2$ added was increased from 0.05 to 0.15, ρ and the $Q \times f$ increased because the porosity decreased. By further increasing the amount of TiO$_2$ added to 0.20, ρ and $Q \times f$ decreased due to the existence of MgTi$_2$O$_5$ and the increase in porosity.

The ε_r of the multiphase system was related to the phase composition. However, the polarizability also played an important role in the ε_r of each phase. The polarizability (α_z) of $(1-z)$LiMg$_{1/2}$Ti$_{3/2}$O$_4$–zMg$_2$TiO$_4$ (z decreased from 0.2 to 0) and $(1-m)$LiMg$_{1/2}$Ti$_{3/2}$O$_4$–mLi$_{4/3}$Ti$_{5/3}$O$_4$ (m increased from 0 to positive value) was calculated as follows:

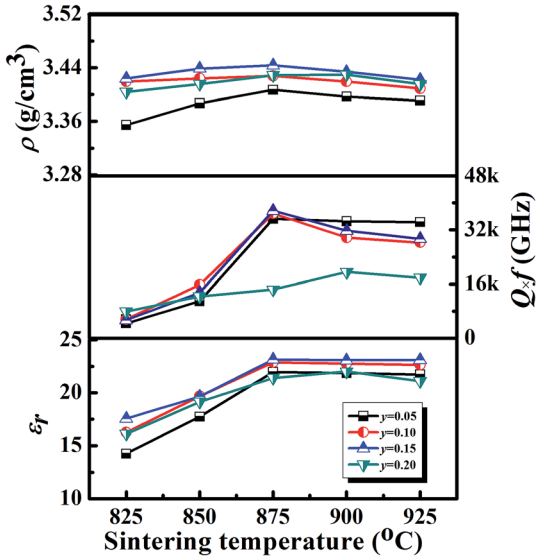

Fig. 5 The bulk density (ρ), permittivity (ε_r) and $Q \times f$ values of the $(1-y)$[0.97LMT–0.03BCB]–yTiO$_2$ (y = 0.05, 0.10, 0.15, 0.20) ceramics as a function of their sintering temperatures.

$$\alpha = x_{Li^+} \times \alpha_{Li^+} + x_{Mg^{2+}} \times \alpha_{Mg^{2+}} + x_{Ti^{4+}} \times \alpha_{Ti^{4+}} + x_{O^{2-}} \times \alpha_{O^{2-}} \quad (2)$$

where x_{Li^+}, $x_{Mg^{2+}}$, $x_{Ti^{4+}}$ and $x_{O^{2-}}$ are the mole numbers of Li^+, Mg^{2+}, Ti^{4+} and O^{2-}, respectively. α_{Li^+}(1.20), $\alpha_{Mg^{2+}}$(1.32), $\alpha_{Ti^{4+}}$(2.93) and $\alpha_{O^{2-}}$(2.01) are the ion dielectric polarizability values of Li^+, Mg^{2+}, Ti^{4+} and O^{2-}, respectively.[23,24] The polarizability values of $(1-z)$LiMg$_{1/2}$Ti$_{3/2}$O$_4$–zMg$_2$TiO$_4$ and $(1-m)$LiMg$_{1/2}$Ti$_{3/2}$O$_4$–mLi$_{4/3}$Ti$_{5/3}$O$_4$ could be expressed as: $\alpha_z = 14.30 - 0.69z$ and $\alpha_m = 14.30 + 0.23m$. α_z increased with decreasing z value and α_m increased with increasing m value. The permittivity (ε_z) of $(1-z)$LiMg$_{1/2}$Ti$_{3/2}$O$_4$–zMg$_2$TiO$_4$ and $(1-m)$LiMg$_{1/2}$Ti$_{3/2}$O$_4$–mLi$_{4/3}$Ti$_{5/3}$O$_4$ could be calculated as follows:

$$\varepsilon_z = \frac{3V_z + 8\pi\alpha_z}{3V_z - 4\pi\alpha_z} = 1 + \frac{12\pi}{\frac{3V_z}{\alpha_z} - 4\pi} \quad (3)$$

where V_z is the molar volume of $(1-z)$LiMg$_{1/2}$Ti$_{3/2}$O$_4$–zMg$_2$TiO$_4$ or $(1-m)$LiMg$_{1/2}$Ti$_{3/2}$O$_4$–mLi$_{4/3}$Ti$_{5/3}$O$_4$.[25,26] For the unit cell parameters of the ceramics, V_z decreased with increasing TiO$_2$ content. The formula (3) shows that the ε_z of $(1-z)$LiMg$_{1/2}$Ti$_{3/2}$O$_4$–zMg$_2$TiO$_4$ (or $(1-m)$LiMg$_{1/2}$Ti$_{3/2}$O$_4$–mLi$_{4/3}$Ti$_{5/3}$O$_4$) increased with increasing α_z (or α_m) and decreasing V_z. The increase of the ε_r of $(1-z)$LiMg$_{1/2}$Ti$_{3/2}$O$_4$–zMg$_2$TiO$_4$ (or $(1-m)$LiMg$_{1/2}$Ti$_{3/2}$O$_4$–mLi$_{4/3}$Ti$_{5/3}$O$_4$) improved the ε_r of $(1-y)$[0.97LMT–0.03BCB]–yTiO$_2$. So, the ε_r increased from 21.9 to 23.1 with increasing the TiO$_2$ content from 0.05 to 0.15. When the TiO$_2$ content increased to 0.20, the ε_r decreased to 22.0, due to the existence of MgTi$_2$O$_5$.

The phase composition is the key factor affecting the τ_f in multiphase systems. The τ_f of $(1-z)$LiMg$_{1/2}$Ti$_{3/2}$O$_4$–zMg$_2$TiO$_4$ increased with a decrease in the z value and the τ_f of $(1-m)$LiMg$_{1/2}$Ti$_{3/2}$O$_4$–mLi$_{4/3}$Ti$_{5/3}$O$_4$ increased with an increase in the m value, because Li$_{4/3}$Ti$_{5/3}$O$_4$ exhibited a positive τ_f (15 ppm °C^{-1}), LiMg$_{1/2}$Ti$_{3/2}$O$_4$ showed a near-zero τ_f (3.2 ppm °C^{-1}) and Mg$_2$TiO$_4$ presented a negative τ_f (−50 ppm °C^{-1}).[27,28] With increasing the y value from 0.05 to 0.15, the τ_f increased from −21.1 ppm °C^{-1} to −5.9 ppm °C^{-1}, because the τ_f of $(1-z)$LiMg$_{1/2}$Ti$_{3/2}$O$_4$–zMg$_2$TiO$_4$ and $(1-m)$LiMg$_{1/2}$Ti$_{3/2}$O$_4$–mLi$_{4/3}$Ti$_{5/3}$O$_4$ increased. However, the τ_f decreased to −15 ppm °C^{-1} due to the existence of MgTi$_2$O$_5$, which had a negative τ_f when y was increased to 0.20.[29]

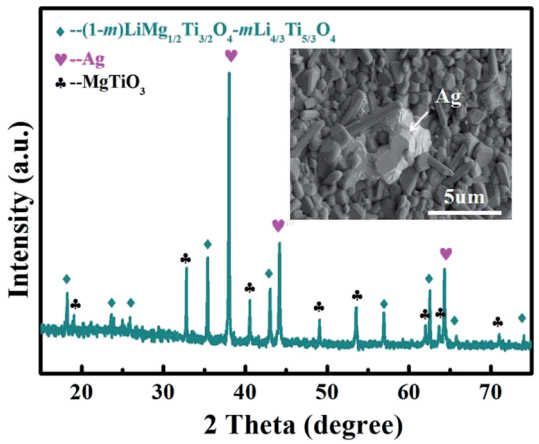

Fig. 6 XRD pattern and backscattered electron image of 0.85[0.97LMT–0.03BCB]–0.15TiO$_2$ with 20 wt% Ag powder sintered at 875 °C.

The 0.85[0.97LMT–0.03BCB]–0.15TiO$_2$ ceramic sintered at 875 °C exhibited good properties with a small ρ of 3.42 g cm^{-3}, high $Q \times f$ of 37 700 GHz, moderate ε_r of 23.1 and near-zero τ_f of −5.9 ppm °C^{-1}, satisfying the requirements of microwave devices, such as a light weight, low loss, miniaturization and high stability. To identify whether the 0.85[0.97LMT–0.03BCB]–0.15TiO$_2$ ceramic could be used in LTCC, the chemical compatibility between the 0.85[0.97LMT–0.03BCB]–0.15TiO$_2$ ceramic and Ag powders was investigated. An XRD pattern and a backscattered electron image of 0.85[0.97LMT–0.03BCB]–0.15TiO$_2$ with 20 wt% Ag powder sintered at 875 °C are displayed in Fig. 6. The results show that the 0.85[0.97LMT–0.03BCB]–0.15TiO$_2$ ceramic did not react with the Ag powder. The 0.85[0.97LMT–0.03BCB]–0.15TiO$_2$ ceramic show good chemical compatibility with Ag. The results indicate that the 0.85[0.97LMT–0.03BCB]–0.15TiO$_2$ ceramic is a good commercial LTCC material.

4. Conclusion

LMT ceramics have been prepared using a solid-state reaction method and excellent microwave dielectric properties were obtained in ceramics sintered at 1100 °C. The addition of BCB could reduce the sintering temperature of the ceramics to 900 °C. TiO$_2$ was introduced to improve the ε_r and τ_f values. The $Q \times f$, ε_r and τ_f values firstly increased and then decreased with increasing the TiO$_2$ content. The 0.85[0.97LMT–0.03BCB]–0.15TiO$_2$ ceramic exhibited a low sintering temperature (~875 °C), good microwave dielectric properties ($Q \times f$ = 37 700 GHz, ε_r = 23.1 and τ_f = −5.9 ppm °C^{-1}) and chemical

compatibility with silver powder, indicating that it is a promising candidate material for LTCC devices.

Conflicts of interest

There are no conflicts to declare.

Acknowledgements

This work was supported by Natural Science Foundation of China (No. 11464009, 61761015, 11664008 and 11364012), Natural Science Foundation of Guangxi (No. 2015GXNSFDA139033), and Project of Outstanding Young Teachers' Training in Higher Education Institutions of Guangxi.

References

1 D. Zhou, W. B. Li, H. H. Xi, L. X. Pang and G. S. Pang, *J. Mater. Chem. C*, 2015, **3**, 2582.
2 K. C. Li, H. Wang and H. F. Zhou, *Int. J. Appl. Ceram. Technol.*, 2010, **7**, E144.
3 W. Lei, W. Z. Lu and X. C. Wang, *Ceram. Int.*, 2012, **38**, 99.
4 H. L. Pan, Q. Q. Liu, Y. H. Zhang and H. T. Wu, *RSC Adv.*, 2016, **6**, 86889.
5 H. Wu and E. S. Kim, *RSC Adv.*, 2016, **6**, 47443.
6 J. R. Kim, D. W. Kim, H. S. Jung and K. S. Hong, *J. Eur. Ceram. Soc.*, 2006, **26**, 2105.
7 Y. G. Zhao and P. Zhang, *RSC Adv.*, 2015, **5**, 97746.
8 X. Y. Du, H. Su, H. W. Zhang, X. T. Liu and X. L. Tang, *RSC Adv.*, 2017, **7**, 27415.
9 G. G. Yao, P. Liu and H. W. Zhang, *J. Mater. Sci.: Mater. Electron.*, 2013, **24**, 1128.
10 C. L. Huang and S. S. Liu, *J. Alloys Compd.*, 2009, **471**, L9.
11 C. Pei, G. Yao, P. Liu and J. Zhou, *Mater. Lett.*, 2016, **184**, 57.
12 Z. Zhou, H. Su, X. Tang and H. Zhang, *Ceram. Int.*, 2016, **42**, 11161.
13 Z. H. Yao, H. X. Liu and Z. Y. Shen, *Mater. Res. Bull.*, 2006, **41**, 1972.
14 J. J. Bian, Q. Yu and J. J. He, *J. Eur. Ceram. Soc.*, 2017, **37**, 647.
15 H. F. Zhou, H. Wang, Y. H. Chen, K. C. Li and X. Yao, *Mater. Chem. Phys.*, 2009, **113**, 1.
16 J. B. Lim, K. H. Cho and S. Nahm, *Mater. Res. Bull.*, 2006, **41**, 1868.
17 X. Tang, H. Yang, Q. L. Zhang and J. H. Zhou, *Ceram. Int.*, 2014, **40**, 12875.
18 Z. Q. Yuan, B. Liu, X. Q. Liu and X. M. Chen, *RSC Adv.*, 2016, **6**, 96229.
19 X. W. Jiang, L. Fang, H. C. Xiang and H. H. Guo, *Ceram. Int.*, 2015, **41**, 13878.
20 J. J. Bian, K. Yan and H. B. Gao, *Mater. Chem. Phys.*, 2006, **96**, 349.
21 S. Wu, K. Song, P. Liu, H. Lin and F. Zhang, *J. Am. Ceram. Soc.*, 2015, **98**, 1842.
22 M. H. Kim, J. B. Lim, J. C. Kim and S. Nahm, *J. Am. Ceram. Soc.*, 2006, **89**, 3124.
23 H. I. Hsiang and S. H. Chung, *J. Alloys Compd.*, 2008, **465**, 356.
24 R. D. Shannon, *J. Appl. Phys.*, 1993, **73**, 348.
25 Y. C. Chen, H. M. You and K. C. Chang, *Ceram. Int.*, 2014, **41**, 5257.
26 H. L. Pan, Q. Q. Liu, Y. H. Zhang and H. T. Wu, *RSC Adv.*, 2016, **6**, 86889.
27 R. K. Bhuyan, T. S. Kumar and D. Goswami, *Mater. Sci. Eng., B*, 2013, **178**, 471.
28 W. Li, *J. Alloys Compd.*, 2017, **701**, 295.
29 V. M. Ferreira, F. Azough and R. Freer, *J. Mater. Res.*, 1997, **12**, 3293.